THE JOURNAL OF PHYSICAL CHEMISTRY C

ARTICLE

pubs.acs.org/JPCC

Time-Dependent Theory of the Rate of Photo-induced Electron Transfer

Hanning Chen, Mark A. Ratner, and George C. Schatz*

Argonne-Northwestern Solar Energy Research Center, Department of Chemistry, Northwestern University, 2145 Sheridan Road, Evanston, Illinois 60208, United States

ABSTRACT: A novel approach based on constrained real-time time-dependent density functional theory (C-RT-TDDFT) is introduced to accurately evaluate the electronic Hamiltonian coupling associated with photoinduced electron transfer (PIET) using diabatic states that are defined using constrained DFT (C-DFT). In combination with the semiclassical Marcus theory, the photoexcited ET rate for coherently coupled photoexcitation and electron transfer is determined for a given incident wavelength by combining this Hamiltonian coupling with free energy changes and ground state reorganization energies that are obtained using an implicit solvation model. As an application of this method, we consider PIET for the $(Ag_{20}-Ag)^+$ complex as a model of a plasmon-enhanced electron transfer process. Using solar radiation intensity, the fastest PIET rate is found to be induced by an incident wavelength that is distinct (blue-shifted) from the wavelength of strongest plasmon-like excitation associated with the Ag_{20}^+ cluster, particularly for large donor−acceptor separations, which suggests a much more efficient coupling Hamiltonian for higher-energy molecular orbitals. Through a comparison between the PIET and absorption cross sections, the quantum efficiency for PIET is found to be a few percent at most at short donor−acceptor distances, and it decays exponentially as they separate.

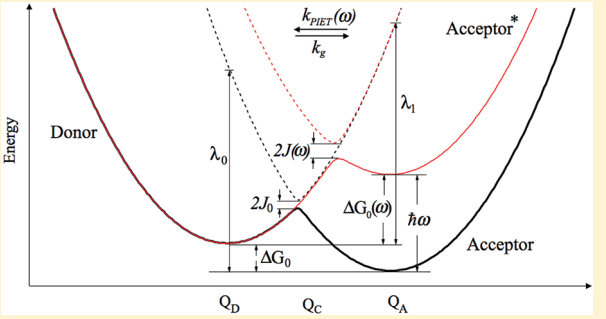

1. INTRODUCTION

Electrons are such mobile elementary particles[1] that their spatial movement in condensed phases from one host species to another can either be driven by internal thermal fluctuations[2] or by external electromagnetic excitation.[3] Often the efficiency and controllability of electron transfer (ET) is of vital importance to essential biological functions of living organisms.[4] One example is the oxidation of the Cytochrome c heme protein[5] that helps to establish a transmembrane proton concentration gradient for adenosine triphosphate (ATP) synthase.[6] In this system, electron release from the heme protein to molecular oxygen is catalyzed by Cytochrome c oxidase (CcO), a terminal enzyme in the respiratory chain of mitochondria.[7] Interestingly, an autocatalytic cycle is formed in this redox reaction through a conformational change in the CcO upon reduction of its bound heme group,[8] suggesting a strong interplay between nuclear motions of the reaction centers and electron transmission through molecular interfaces.[9,10] Another instance of pronounced vibration-electronic coupling arises in inelastic electron tunneling across single-molecule transistors at very low temperature,[11,12] where the transferred electron can lose one quantum of vibrational energy at the molecular junction. In this case, the onset of a small conductance increase is only observed when the biased chemical potential between the two electrodes is larger than the junction's vibrational quanta, leading to a discontinuity in the first derivative of the current−voltage ($I-V$) curve, better represented as a peak in the second derivative of an $I-V$ graph.[13] In fact, even at zero temperature, the ET is not completely suppressed thanks to the zero-point fluctuations.[14]

Another typically more efficient way to promote ET is through light irradiation,[15] wherein the ET donor is excited to a higher electronic state followed by transfer of an electron to the ET acceptor through vibronic coupling.[16] The improved efficiency of photoinduced electron transfer (PIET) over thermally activated ET has been largely ascribed to stronger electronic coupling between the donor excited state and the acceptor ground state than between the ground states,[17,18] because the excited state wave function is generally much more diffuse than its ground state counterpart.[19] It is also found that ET can even occur without direct orbital overlap between a donor and an acceptor, in contrast with the Dexter exchange quenching mechanism.[20] In order to explain the long-distance charge transfer between two phenyl groups linked by a polymethylene chain,[21] the so-called "superexchange" mechanism[22] was introduced, based upon wave function mixing with virtual states of the spacer molecules. The perspective of "superexchange" has gained extensive support from studies of donor-bridge-acceptor (DBA) systems,[23,24] in which the PIET rate is usually observed to decay exponentially with donor−acceptor separation.[25,26] Although a larger free

Received: June 4, 2011
Revised: August 2, 2011
Published: August 12, 2011

energy difference between donor and acceptor does not always ensure a faster charge transfer,[27,28] it is nevertheless an essential factor as demonstrated by the strong dependence of the PIET rate on the size-modulated injection potential in a quantum dot-metal oxide junction.[29] In addition, the ease of solvent reorientation upon charge transfer relative to the transient lifetime of the excited species is also widely believed to be critical to PIET.[30,31]

The standard Marcus expression for the electron transfer rate is[32]

$$k_{ET} = \frac{2\pi}{\hbar}|H_{DA}|^2 \frac{1}{\sqrt{4\pi\lambda k_B T}} e^{-(\Delta G_0 + \lambda)^2/4\lambda k_B T} \quad (1)$$

where H_{DA} is the electronic coupling strength, λ is the reorganization energy, ΔG_0 is the free energy difference between donor and acceptor, and T is the absolute temperature. This expression assumes that the vibrational states are governed by a classical Boltzmann distribution (i.e., $\hbar\omega_{vib} \ll k_B T$). In the Born−Oppenheimer approximation, the vibronic wave function, $\Psi(R,r)$, is separable into a nuclear part, $\varphi_N(R)$, and an electronic part, $\psi_e(r)$:

$$\Psi(R,r) = \varphi_N(R)\psi_e(r) \quad (2)$$

So, eq 1 includes a density-weighted Franck−Condon (DWFC) factor, $(1/(4\pi\lambda k_B T)^{1/2})e^{-(\Delta G_0 + \lambda)^2/(4\lambda k_B T)}$, which arises from the vibrational orbital overlap, $\langle\varphi_N(D)|\varphi_N(A)\rangle$, between the donor (D) and the acceptor (A), and an electronic coupling Hamiltonian term H_{DA} given by

$$H_{DA} = \langle\psi_e(D)|\hat{H}_0|\psi_e(A)\rangle \quad (3)$$

For ET assisted by high-frequency molecular vibrations with $\hbar\omega_{vib} \gg k_B T$, the more generally applicable Marcus−Dogonadze−Jortner equation accounts for nuclear tunneling effects:[33]

$$k_{ET} = \frac{|H_{DA}|^2}{\hbar}\sqrt{\frac{\pi}{\lambda k_B T}}\sum_{j=0}^{\infty}\left(\frac{e^{-D}}{j!}D^j\right)e^{-(\Delta G_0 + \lambda + j\hbar\omega_{vib})^2/4\lambda k_B T} \quad (4)$$

where D is the vibrational-electronic coupling strength, a simple function of the reduced bond strength change. Because the present study is restricted to the study of PIET induced by the slow solvent reorientation, our methodology development and the discussions thereafter will be exclusively based on eq 1, the reduced semiclassical form of Marcus theory. Thus, the nonadiabatic ET rate is readily determined once three key factors, namely H_{DA}, λ, and ΔG_0, are known.

For decades, a challenging task with the theoretical modeling of ET has been the reliable construction of the diabatic ET states[34,35] in which charge is localized on one of the two reaction centers.[36] Recently, constrained density functional theory (C-DFT) has been developed, which provides this capability through the imposition of a desired charge constraint onto the position-dependent Hartree potential.[37] Although C-DFT still suffers from the self-interaction error (SIE) within each constrained region (which is a well-known deficiency of DFT[38] particularly for strongly correlated electronic systems[39]), it was fairly successful in applications to charge recombination rates for anthraquinone dye molecules[36] and to the exchange-coupling constants of transition-metal complexes.[40] As an added benefit for our calculation of long-range ET, C-DFT directly builds the charge-transfer (CT) state, in which the energy of the lowest unoccupied molecular orbital (LUMO) can be regarded as the electron affinity.[41] By contrast, only the highest occupied molecular orbital (HOMO) energy is meaningful in conventional DFT through the use of the ground state as the reference state, as there is a energy discontinuity with respect to electron number.[42] It is also known that when the donor and the acceptor are spatially well separated, the soundness of time-dependent density functional theory (TDDFT)[43] is questionable due to the negligible orbital overlap if the popular local exchange-correlation functionals are used.[44] Consequently, C-DFT is seemingly a promising solution for tackling the longstanding issue of the underestimated excitation energy in TDDFT[45] which can result in incorrect values for the ET driving force.

Real-time time-dependent density functional theory (RT-TDDFT), a time-domain variant of TDDFT, has received increasing attention since its first application in calculating the dipole response of large atomic clusters in an external perturbing electric field.[46] In concert with rapid developments in laser technology using ultrashort pulses and intense power,[47] RT-TDDFT enables the direct study of electron dynamics in a computationally feasible manner.[48] The common practice of RT-TDDFT is to numerically solve the time-dependent Kohn−Sham equation[49] subject to an electric dipole interaction that includes a time-dependent external electromagnetic field. Because RT-TDDFT allows for an arbitrary number of external perturbations, both linear[50] and nonlinear[51] optical properties can handily be incorporated within same theoretical framework by solving coupled dipole-field response equations. A hybrid quantum mechanics/classical electrodynamics (QM/ED) approach was recently formulated to account for the polarization effect of a nanoparticle on the optical properties of a nearby dye molecule.[52] Besides flexibility and extensibility, RT-TDDFT is also noted for its smaller basis set requirements as it avoids explicit construction of the unoccupied (virtual) molecular orbitals.[53] In most cases, a basis set sufficient for a ground state calculation can be adopted for RT-TDDFT, and in the presence of a modest light source (such as solar radiation) there is only a small fluctuation around the optimized ground state wave function. Another attractive feature of RT-TDDFT is its capability to determine any linear physical property over a broad range of incident frequencies from a single simulation.[54] This allows for systematic design of dye molecules with desired optical properties, including PIET.

Despite considerable efforts devoted to the description of ET in both closed[53,55] and open[56,57] systems using RT-TDDFT, the simulation duration is still severely limited by the computational cost associated with the explicit electron dynamics. Therefore, only ET phenomena associated with a few hundred femtoseconds of simulation can be simulated by RT-TDDFT. However for PIET processes involving plasmonic nanoparticles, which comprise the application of interest in this paper, this time limitation is not a problem as plasmon relaxation occurs on this same time scale.

Another theoretical difficulty with using RT-TDDFT to model ET arises in the construction of the initial and final electronic states, which typically are not eigenstates of the full electronic Hamiltonian.[41,58] In earlier work, a RT-TDDFT study was carried out to track the molecular conductance across a polyacetylene wire after a chemical potential bias had been established through an electron density gradient that was generated by a charge constraint.[59] Although steady state electron transmission was never reached in that study due to the

persistently decreasing bias voltage, the idea of incorporating C-DFT into RT-TDDFT calculations to define diabatic ET is an important suggestion. Another encouraging attempt to treat the photon-phonon coupling was made in the description of excited carrier dynamics in a carbon nanotube. Here C-DFT was employed to build an initial excited state to mimic photoexcitation and then an Ehrenfest molecular dynamics (EMD) calculation was used to describe nonradiative decay leading to charge density variation.[60] However, an issue with the combined C-DFT/EMD approach is that it is not always easy to identify the appropriate charge constrained states as the initial condition in EMD leads to considerable uncertainty about the excitation energy generated by DFT.[44] For example, the energy-level degeneracy of the excited states can impose ambiguity.

In light of the growing interest in modeling PIET, a reliable and feasible first-principle approach is needed for evaluating electron transfer rates that are important in numerous applications, including high-efficiency solar cells,[61] photoconductive molecular electronics[62] and photocatalytic water splitting.[63] We herein present a time-dependent formalism to evaluate the PIET rate within the framework of Marcus ET theory.[64] A novel component of our work is the rigorous determination of the Hamiltonian coupling matrix element between the excited charge transfer state and the diabatic ground state by tracking their time-dependent wave function overlap along a RT-TDDFT trajectory. During a RT-TDDFT simulation, a constrained position-dependent Hartree potential is applied not only to construct the initial diabatic wave function, but also to guide the electron dynamics with the diabatic Hamiltonian. The emphasis in this work is on plasmonic PIET processes, so we only consider short-time coherent dynamics that can occur before plasmon relaxation occurs on the 10−100 fs time scale. This relaxation is included using empirical damping factors, and the nuclei are assumed fixed. Generalizations to include nuclear motions are possible, but will not be considered.

The remainder of this paper is organized as follows. In section 2, the protocol to calculate the ground state electron transfer rate is introduced based on the C-DFT, an implicit solvation model and the Marcus formalism. In section 3, the constrained real-time time-dependent density functional theory (C-RT-TDDFT) is formulated to determine the frequency-dependent PIET matrix element that will be used to evaluate the PIET rate and the excited state ET rate. In section 4, we report numerical results for a model plasmonic system, the complex $(Ag_{20}-Ag)^+$, consisting of a Ag_{20} cluster and an isolated Ag atom, which we use to study the correlation between photoabsorption and photoinduced electron transfer. Finally, we summarize our results and briefly discuss possible applications in section 5.

2. GROUND STATE ELECTRON TRANSFER RATE, k_g

As illustrated in Figure 1, PIET within a closed system can be simplified to a cyclic three-state process (here with spin-forbidden intersystem crossing[65] and excited state decay[66] being neglected). In this picture, the three states are the ground donor (D), the ground acceptor (A) and the excited acceptor (A*), and the three transition paths between these diabatic states are vertical excitation, excited state ET and ground state ET. Please note that we have assumed that the ground state acceptor is below the ground state donor, while excited state acceptor is above ground state donor. Excitation of the ground donor is not considered due to its relatively low population in comparison to

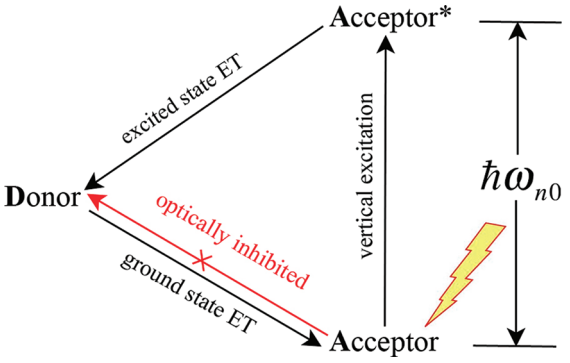

Figure 1. Energy level diagram which shows the relationship of photoinduced electron transfer to ground state ET. $\hbar\omega_{n0}$ is the vertical excitation energy.

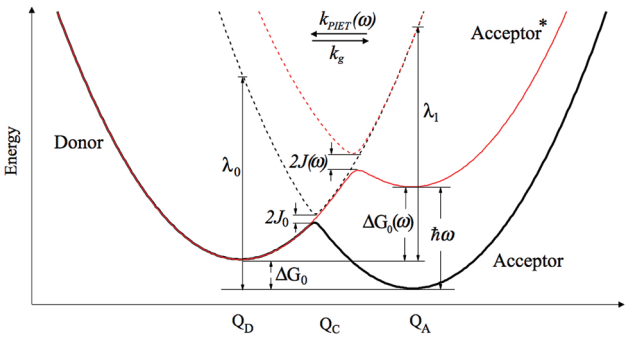

Figure 2. Energy level diagram for ground state ET and excited state ET.

the ground acceptor. Also, the thermal acceptor to donor rate is assumed to be very slow and is thus neglected.

In ET theory, the diabatic states are defined by imposing charge localization on the reaction centers.[58] In this sense, the atomic charge distribution, Q_C, of a given diabatic state must satisfy the definition of that diabatic state:

$$Q_C = \hat{Q}(\psi_e(R,r)) \tag{5}$$

where $\hat{Q}$ is an operator to transform the delocalized electronic wave function into localized atomic charges. Upon ET, there is an associated free energy change, ΔG_0, (Figure 2) which receives contributions from both the reactive system and from the surrounding environment, e.g., solvent:

$$\Delta G_0 = \Delta G_{0,\text{intra}} + \Delta G_{0,\text{sol}} \tag{6}$$

In this paper, the entropy component of eq 6 is ignored due to the use of an implicit solvent model. Accordingly, ΔG_0 can be rewritten as

$$\Delta G_0 = (E_A - E_D) + \left(\sum_{i=1}^{N} U_{A,i}Q_{A,i} - \sum_{i=1}^{N} U_{D,i}Q_{D,i}\right) \tag{7}$$

where E_D and E_A are the energies of the donor and acceptor and $U_{D,i}$ and $U_{A,i}$ are the solvation potentials acting on the ith atom. The latter can be determined by solving the Poisson equation

$$\nabla\cdot[\varepsilon(r)\nabla U(r)] = -4\pi Q(r) \tag{8}$$

where ε is the position-dependent dielectric constant and $Q(r)$ are the atomic charges derived from the C-DFT calculations.

Similarly, another essential parameter of ground state ET, λ_0, is evaluated as

$$\lambda_0 = \left(\sum_{i=1}^{N} U_{D,i}Q_{A,i} - \sum_{i=1}^{N} U_{A,i}Q_{A,i}\right) \quad (9)$$

to reflect the energy penalty of solvent reorientation.

Following the C-DFT protocol presented by Wu and Van Voorhis,[67] the procedure to calculate the electronic Hamiltonian matrix element, H_{DA}, is briefly summarized as follows:

(i) A constrained energy minimization with respect to electron density is performed for each of the desired Q_D and Q_A to determine the charge-constrained states of ψ^0_{CD} and ψ^0_{CA}, respectively:

$$(\hat{H}_0 + V_C\hat{w}_C)\psi^0_C = F_C\psi^0_C \quad (10)$$

where both the constraining strength, V_C, and the constraining operator, $\hat{w}_C$ are unique for a given Q_C. Additionally, $\hat{H}_0$ is the standard DFT Hamiltonian that includes the kinetic energy, Coulomb repulsion, ion-electron attraction, and exchange-correlation term.[68]

(ii) Since ψ^0_{CD} and ψ^0_{CA} are not guaranteed to be orthogonal, a diagonalization of the overlap matrix

$$S = \begin{pmatrix} 1 & \langle\psi^0_{CD}|\psi^0_{CA}\rangle \\ \langle\psi^0_{CA}|\psi^0_{CD}\rangle & 1 \end{pmatrix}$$

is needed to determine the diabatic transformation matrix C

$$w_C C = SCN \quad (11)$$

where

$$w_C = \begin{pmatrix} Q_D & \langle\psi^0_{CD}|\hat{w}_C|\psi^0_{CA}\rangle \\ \langle\psi^0_{CA}|\hat{w}_C|\psi^0_{CD}\rangle & Q_A \end{pmatrix}$$

is the constraining matrix and N is a diagonal matrix.

(iii) The true diabatic ground states with strict orthogonality, i.e., $\langle\psi^0_A|\psi^0_D\rangle = 0 = \langle\psi^0_D|\psi^0_A\rangle$, are constructed from ψ^0_{CD} and ψ^0_{CA} with the aid of the Hermitian transpose of the matrix C

$$\begin{pmatrix} \psi^0_D \\ \psi^0_A \end{pmatrix} = C^\dagger \begin{pmatrix} \psi^0_{CD} \\ \psi^0_{CA} \end{pmatrix} \quad (12)$$

Finally, the ground state diabatic Hamiltonian coupling matrix element, H^0_{DA} is the off-diagonal term of the resultant matrix

$$C^\dagger \begin{pmatrix} E_D & F_A\langle\psi^0_{CD}|\psi^0_{CA}\rangle - V^A_C\langle\psi^0_{CD}|\hat{w}^A_C|\psi^0_{CA}\rangle \\ F_D\langle\psi^0_{CA}|\psi^0_{CD}\rangle - V^D_C\langle\psi^0_{CA}|\hat{w}^D_C|\psi^0_{CD}\rangle & E_A \end{pmatrix} C \quad (13)$$

With ΔG_0, λ_0, and H^0_{DA} on our hands, we are in a good position to calculate k_g using eq 1 if the temperature is high enough for a sufficient population in the vibrational states of the diabatic potential well (Figure 2).

3. PHOTOINDUCED ELECTRON TRANSFER RATE, $k_{PIET}(\omega)$

Assuming the absence of structural relaxation upon electronic excitation, the PIET driving force and reorganization energy are given by

$$\Delta G_0(\omega) = -\Delta G_0 - \hbar\omega \quad (14)$$

and

$$\lambda_1 = \left(\sum_{i=1}^{N} U_{A,i}Q_{D,i} - \sum_{i=1}^{N} U_{D,i}Q_{D,i}\right) \quad (15)$$

where ω is the incident light angular frequency.

For a system under a time-dependent Hamiltonian, $\hat{H}_1(t)$, its time evolution operator, $\hat{U}(t_0,t)$, follows the time-dependent Schrödinger equation

$$i\hbar\frac{\partial\hat{U}(t_0,t)}{\partial t} = (\hat{H}_0 + \hat{H}_1(t))\hat{U}(t_0,t) \quad (16)$$

and it can be separated into a stationary part, $\hat{U}_0(t_0,t)$, and a perturbative part, $\hat{U}_1(t_0,t)$

$$\hat{U}(t_0,t) = \hat{U}_0(t_0,t)\hat{U}_1(t_0,t) \quad (17)$$

where

$$\hat{U}_0(t_0,t) = e^{-i\hat{H}_0(t-t_0)/\hbar} \quad (18)$$

With the boundary condition

$$\hat{U}(t_0,t_0) = 1 \quad (19)$$

it is easy to recognize that

$$\hat{U}_1(t_0,t) = 1 - \frac{i}{\hbar}\int_{t_0}^{t} dt'\, e^{i\hat{H}_0(t-t_0)/\hbar}\hat{H}_1(t')e^{-i\hat{H}_0(t-t_0)/\hbar}\hat{U}_1(t_0,t') \quad (20)$$

Therefore, $\hat{U}_1(t_0,t)$ can be expanded to any order in a recursive manner

$$\hat{U}_1(t_0,t) = 1 - \frac{i}{\hbar}\int_{t_0}^{t} dt'\, e^{i\hat{H}_0(t-t_0)/\hbar}\hat{H}_1(t')e^{-i\hat{H}_0(t-t_0)/\hbar} \times \left(1 - \frac{i}{\hbar}\int_{t_0}^{t} dt'\, e^{i\hat{H}_0(t-t_0)/\hbar}\hat{H}_1(t')e^{-i\hat{H}_0(t-t_0)/\hbar}\hat{U}_1(t_0,t')\ldots\right) \quad (21)$$

If a system's wave function is expressed as a linear combination of the eigenstates of the constrained Hamiltonian, $\hat{H}_0 + V_c\hat{w}_c$

$$\Psi(t) = \sum_n c_n(t)\Psi_n e^{-iE_nt/\hbar} \quad (22)$$

The coefficient of a given diabatic state, Ψ_n, follows the Dyson series

$$c_n(t) = c_n^{(0)} + c_n^{(1)} + c_n^{(2)} + \ldots \quad (23)$$

dx.doi.org/10.1021/jp205262u |J. Phys. Chem. C 2011, 115, 18810–18821

where

$$c_n^{(0)} = \delta_{0n}$$

$$c_n^{(1)} = -\frac{i}{\hbar}\int_{t_0}^{t'} dt' \langle \Psi_n|\hat{H}_1(t')|\Psi_0\rangle e^{i\omega_{n0}(t'-t_0)}$$

$$c_n^{(2)} = (-\frac{i}{\hbar})^2 \sum_m \int_{t_0}^{t} dt' \langle \Psi_n|\hat{H}_1(t')|\Psi_m\rangle e^{i\omega_{nm}(t'-t_0)} \times \int_{t_0}^{t'} dt'' \langle \Psi_m|\hat{H}_1(t'')|\Psi_0\rangle e^{i\omega_{m0}(t''-t_0)}$$

... (24)

In the context of PIET (Figure 1), Ψ_0 is the ground acceptor state, Ψ_m refers to all Franck−Condon allowed excited states within the acceptor manifold, and Ψ_n represents the ground donor state, Ψ_D. The coupling Hamiltonian $\hat{H}_1(t)$ is the sum of the full Hamiltonian $\hat{H}_0$ (which leads to diabatic coupling) and the dipole interaction $\vec{E}_x(t)\cdot\vec{\mu}_x$.

In the small perturbation limit, Ψ_D can be added to the basis set used to represent $\Psi(t)$ due to the assumptions

$$\langle\Psi_0|\Psi_D\rangle = 0 \text{ and } c_n(t)\approx 0 \ (n \neq 0) \quad (25)$$

In addition, $c_n^{(1)}(t)$, which refers to the "direct transition" from Ψ_0 to Ψ_D can be taken to be zero, as there is no diabatic coupling between these states due to eq 25 and their optical coupling is neglected as discussed previously. As a result, the first nonzero term in eq 24 involves $c_n^{(2)}(t)$, corresponding to the "indirect transition" between Ψ_0 and Ψ_D via the intermediate state, Ψ_m. In this evaluation, the coupling matrix element between Ψ_0 and Ψ_m is within the acceptor manifold is therefore based on constrained states. This matrix element arises from the dipole interaction, while the coupling Ψ_m and Ψ_D is between acceptor and donor manifolds and therefore involves the diabatic coupling.

Using the same notation as in section 2, Ψ_0 and Ψ_D are $\varphi_A(R)\psi_A^0(R,r)$ and $\varphi_D(R)\psi_D^0(R,r)$ respectively. To simplify the Franck−Condon factor evalution, we assume that the only excited states, Ψ_m, that contribute to the PIET process have the same initial vibrational wave function as Ψ_0, i.e.

$$\Psi_m(t_0) = \varphi_A(R,t_0)\psi_m(R,r) \quad (26)$$

If a continuous wave, $E_x(e^{i\omega t} + e^{-i\omega t})$, is turned on at $t_0 = 0$ to vertically excite the system, then the matrix element of $\hat{H}_1(t)$ between ground and excited states within the acceptor manifold is

$$\langle\Psi_m|\hat{H}_1(t')|\Psi_0\rangle = \langle\psi_m|\vec{E}_x\cdot\vec{\mu}_x|\psi_A^0\rangle(e^{i\omega t} + e^{-i\omega t}) \quad (27)$$

Similarly the matrix element of $\hat{H}_1(t)$ between Ψ_m and Ψ_D involves the diabatic coupling

$$\langle\Psi_D|\hat{H}_0|\Psi_m\rangle = \langle\psi_D^0|\hat{H}_0|\psi_m\rangle\langle\varphi_D|\varphi_A\rangle \quad (28)$$

By inserting eqs 27 and 28 into eq 24, the second-order Dyson coefficient of the donor state is given by

$$\begin{aligned} c_D^{(2)} &= \left(-\frac{i}{\hbar}\right)^2 \sum_m \int_0^t dt' \langle\Psi_D|\hat{H}_0|\Psi_m\rangle e^{i\omega_{md}t'} \int_{t_0}^{t'} dt'' (e^{i\omega t''} + e^{-i\omega t''})\langle\Psi_m|\vec{E}_x\cdot\vec{\mu}_x|\Psi_0\rangle e^{i\omega_{m0}t''} \\ &= \left(-\frac{i}{\hbar}\right)^2 \sum_m \int_0^t dt' \langle\varphi_D|\varphi_A\rangle\langle\psi_D^0|\hat{H}_0|\psi_m\rangle e^{i\omega_{md}t'} \times \int_{t_0}^{t'} dt'' (e^{i\omega t''} + e^{-i\omega t''})\langle\psi_m|\vec{E}_x\cdot\vec{\mu}_x|\psi_A^0\rangle e^{i\omega_{m0}t''} \\ &= \left(-\frac{i}{\hbar}\right)^2 \sum_m \langle\psi_D^0|\hat{H}_0|\psi_m\rangle\langle\psi_m|\vec{E}_x\cdot\vec{\mu}_x|\psi_A^0\rangle\langle\varphi_D|\varphi_A\rangle \times \int_0^t dt' e^{i\omega_{md}t'}\left(\frac{e^{i(\omega_{m0}+\omega)t'}-1}{i(\omega_{m0}+\omega)} - \frac{e^{i(\omega_{m0}-\omega)t'}-1}{i(\omega_{m0}-\omega)}\right) \\ &= \left(-\frac{i}{\hbar}\right)^2 \sum_m \langle\psi_D^0|\hat{H}_0|\psi_m\rangle\langle\psi_m|\vec{E}_x\cdot\vec{\mu}_x|\psi_A^0\rangle\langle\varphi_D|\varphi_A\rangle \times \left(\frac{e^{i(\omega_{d0}+\omega)t}-1}{(\omega_{m0}+\omega)(\omega_{d0}+\omega)} - \frac{e^{i\omega_{dm}t}-1}{(\omega_{m0}+\omega)\omega_{dm}} + \frac{e^{i(\omega_{d0}-\omega)t}-1}{(\omega_{m0}-\omega)(\omega_{d0}-\omega)} - \frac{e^{i\omega_{dm}t}-1}{(\omega_{m0}-\omega)\omega_{dm}}\right) \end{aligned} \quad (29)$$

Note that the sum over m in this expression is a restricted sum that only refers to those states that have a Franck−Condon factor of unity.

In the vicinity of $\omega \approx \omega_{m0}$,

$$c_D^{(2)}\approx\left(-\frac{i}{\hbar}\right)^2 \langle\psi_D^0|\hat{H}_0|\psi_m\rangle\langle\psi_m|\vec{E}_x\cdot\vec{\mu}_x|\psi_A^0\rangle\langle\varphi_D|\varphi_A\rangle \times \left(\frac{e^{i(\omega_{d0}-\omega)t}-1}{(\omega_{m0}-\omega)(\omega_{d0}-\omega)} - \frac{e^{i\omega_{dm}t}-1}{(\omega_{m0}-\omega)\omega_{dm}}\right) \quad (30)$$

Accordingly, the time evolution of the electron population at Ψ_D subject to an incident photon energy $\hbar\omega_{m0}$ is

$$\begin{aligned} |c_D|^2 &\approx \left(-\frac{i}{\hbar}\right)^4 \langle\psi_D^0|\hat{H}_0|\psi_m\rangle^2\langle\psi_m|\vec{E}_x\cdot\vec{\mu}_x|\psi_A^0\rangle^2\langle\varphi_D|\varphi_A\rangle^2 \times \left(\frac{e^{i(\omega_{d0}-\omega)t}-1}{(\omega_{m0}-\omega)(\omega_{d0}-\omega)} - \frac{e^{i\omega_{dm}t}-1}{(\omega_{m0}-\omega)\omega_{dm}}\right) \times \left(\frac{e^{-i(\omega_{d0}-\omega)t}-1}{(\omega_{m0}-\omega)(\omega_{d0}-\omega)} - \frac{e^{-i\omega_{dm}t}-1}{(\omega_{m0}-\omega)\omega_{dm}}\right) \\ &= \left(\frac{1}{\hbar}\right)^4 \langle\psi_D^0|\hat{H}_0|\psi_m\rangle^2\langle\psi_m|\vec{E}_x\cdot\vec{\mu}_x|\psi_A^0\rangle^2\langle\varphi_D|\varphi_A\rangle^2 \times \left(\frac{\sin^2\frac{(\omega_{d0}-\omega)t}{2}}{(\omega_{m0}-\omega)^2\left(\frac{\omega_{d0}-\omega}{2}\right)^2} + \frac{\sin^2\frac{\omega_{dm}t}{2}}{(\omega_{n0}-\omega)^2\left(\frac{\omega_{dm}}{2}\right)^2} + \frac{2(\cos(\omega_{d0}-\omega)t + \cos\omega_{dm}t)}{(\omega_{m0}-\omega)^2(\omega_{d0}-\omega)\omega_{dm}} + \frac{\sin^2\frac{(\omega_{m0}-\omega)t}{2}}{\left(\frac{\omega_{m0}-\omega}{2}\right)^2(\omega_{d0}-\omega)\omega_{dm}}\right) \end{aligned} \quad (31)$$

For a continuous band characterized by a density of states, $\rho(\omega_d)$

$$|c_D|^2 = \left(\frac{1}{\hbar}\right)^4 \langle\psi_D^0|\hat{H}_0|\psi_m\rangle^2\langle\psi_m|\vec{E}_x\cdot\vec{\mu}_x|\psi_A^0\rangle^2\langle\varphi_D|\varphi_A\rangle^2 \times \int_{-\infty}^{+\infty} d\omega_{d0}\,\rho(\omega_d) \times \left(\frac{\sin^2\frac{(\omega_{d0}-\omega)t}{2}}{\left(\frac{\omega_{d0}-\omega}{2}\right)^2(\omega_{m0}-\omega)^2} + \frac{\sin^2\frac{\omega_{dm}t}{2}}{(\omega_{m0}-\omega)^2\left(\frac{\omega_{dm}}{2}\right)^2} + \frac{2(\cos(\omega_{d0}-\omega)t + \cos\omega_{dm}t)}{(\omega_{m0}-\omega)^2(\omega_{d0}-\omega)\omega_{dm}} + \frac{\sin^2\frac{(\omega_{m0}-\omega)t}{2}}{\left(\frac{\omega_{m0}-\omega}{2}\right)^2(\omega_{d0}-\omega)\omega_{dm}}\right)$$

$$= \left(\frac{1}{\hbar}\right)^4 \langle\psi_D^0|\hat{H}_0|\psi_m\rangle^2\langle\psi_m|\vec{E}_x\cdot\vec{\mu}_x|\psi_A^0\rangle^2\langle\varphi_D|\varphi_A\rangle^2\frac{2\pi t\rho(\omega_d)}{(\omega_{m0}-\omega)^2}$$

$$\approx\frac{2\pi t}{\hbar}\frac{\langle\psi_D^0|\hat{H}_0|\psi_m\rangle^2\langle\psi_m|\vec{E}_x\cdot\vec{\mu}_x|\psi_A^0\rangle^2}{\Gamma^2}\frac{\langle\varphi_D|\varphi_A\rangle^2\rho(\omega_d)}{\hbar} \quad (32)$$

where an empirical damping factor of Γ is added to the resonance energy, i.e., $\hbar\omega_{m0} \rightarrow \hbar\omega_{m0} + i\Gamma$, to reflect the broadening of the resonance peak due to the quantum dephasing and vibronic coupling. In combination with the density-weighted Franck−Condon factor between the potential energy surfaces of ψ_D^0 and ψ_m as derived by Marcus,[32] the PIET rate equals

$$k_{PIET}(\omega) = \frac{d|c_D|^2}{dt} = \frac{2\pi}{\hbar}\frac{\langle\varphi_D|\varphi_m\rangle^2\rho(\omega_d)}{\hbar}\frac{\langle\psi_D^0|\hat{H}_0|\psi_m\rangle^2\langle\psi_m|\vec{E}_x\cdot\vec{\mu}_x|\psi_A^0\rangle^2}{\Gamma^2}$$

$$= \frac{2\pi}{\hbar}(DWFC)_{dm}\frac{\langle\psi_D^0|\hat{H}_0|\psi_m\rangle^2\langle\psi_m|\vec{\mu}_x|\psi_A^0\rangle^2}{\Gamma^2}\frac{I(\omega)}{c\varepsilon_0} \quad (33)$$

where c is the speed of light, ε_0 is the vacuum permittivity, $I(\omega)$ is the radiation intensity, and $\langle\psi_D^0|\hat{H}_0|\psi_m\rangle\langle\psi_m|\vec{\mu}_x|\psi_A^0\rangle$ is the absorption-weighted electronic coupling strength.

As might be expected, the PIET rate (eq 33) is proportional to the square of the diabatic coupling matrix element multiplied by the square of the dipole matrix element, and divided by the square of the excited state width. This is consistent with the assumed coherent mechanism in which photoexcitation is directly coupled to electron transfer, and it is only processes which take place during the excited state lifetime that can contribute to the rate.

Inspired by the RT-TDDFT,[54] a numerically convenient way to evaluate $\langle\psi_D^0|\hat{H}_0|\psi_m\rangle^2\langle\psi_m|\vec{\mu}_x|\psi_A^0\rangle^2$ is to track the time evolution of the electronic coupling strength between ψ_D^0 and $\psi_A(t)$ after a short electric pulse of E_x is applied to the acceptor for a time of Δt

$$H_{DA}(t) = \langle\psi_D^0|\hat{H}_0|\psi_A(t)\rangle\approx\langle\psi_D^0|\hat{H}_0|\psi_A^0\rangle + \sum_m c_m(t)\langle\psi_D^0|\hat{H}_0|\psi_m\rangle$$

$$= H_{DA}^0 + \sum_m\frac{-i}{\hbar}\langle\psi_D^0|\hat{H}_0|\psi_m\rangle\Delta t\langle\psi_A^0|\vec{E}_x\cdot\vec{\mu_x}|\psi_m\rangle \times (e^{-i\omega_{m0}t} + e^{i\omega_{m0}t}) \quad (34)$$

Subsequently, a Fourier transform of the perturbative part of $H_{DA}(t)$ at $\omega \approx \omega_{m0}$ normalized by $E_x\Delta t$ yields

$$\mu_{DA,x}(\omega) = \frac{\int dt\Delta\, H_{DA}(t)e^{(i\omega-\Gamma)t}}{\int dt\, E_x} = \frac{\langle\psi_D^0|\hat{H}_0|\psi_m\rangle\Delta t\langle\psi_A^0|\vec{E}_x\cdot\vec{\mu_x}|\psi_m\rangle\rho(\omega)}{\hbar E_x\Delta t}$$

$$\approx\frac{\langle\psi_D^0|\hat{H}_0|\psi_m\rangle\langle\psi_m|\vec{\mu_x}|\psi_A^0\rangle}{\Gamma} \quad (35)$$

where $\mu_{DA,x}$ is defined as the electron transfer matrix element that has the same unit as electric dipole moment. In general, the spatial averaging has to be taken account of for randomly polarized incident light

$$\mu_{DA}(\omega) = \frac{1}{3}(\mu_{DA,x}(\omega) + \mu_{DA,y}(\omega) + \mu_{DA,z}(\omega)) \quad (36)$$

Alternatively, $\Delta H_{DA}(t)$ can be written as

$$\Delta H_{DA}(t) = \langle\psi_D(t)|\hat{H}_0|\psi_A^0\rangle - H_{DA}^0 = \langle\psi_D(t)|\psi_A^0\rangle\langle\psi_A^0|\hat{H}_0|\psi_A^0\rangle + \langle\psi_D(t)|\psi_D^0\rangle\langle\psi_D^0|\hat{H}_0|\psi_A^0\rangle - H_{DA}^0 = \langle\psi_D(t)|\psi_A^0\rangle E_A + \langle\psi_D(t)|\psi_D^0\rangle H_{DA}^0 - H_{DA}^0 \quad (37)$$

In the limit of a small perturbation

$$\langle\psi_D(t)|\psi_D^0\rangle \approx 1 \quad (38)$$

we end up with a concise form for $\Delta H_{DA}(t)$,

$$\Delta H_{DA}(t) = \langle\psi_D^0|\psi_A(t)\rangle E_A \quad (39)$$

Now, the computational task of determining the excited state ET rate has been simplified to an evaluation of the time dependence of the diabatic wave function overlap.

For each of the two charge-constrained states, ψ_{CD}^0 and ψ_{CA}^0 that are determined by C-DFT in eq 10, the perturbation field, E_x, is added to their Hamiltonian. Then, their wave function evolution can be described by solving the time-dependent Kohn−Sham equation

$$i\frac{\partial|\psi_C(t)\rangle}{\partial t} = (\hat{H}_0 + V_C\hat{w}_C + \vec{E}_x\cdot\vec{\mu_x})|\psi_C(t)\rangle \quad (40)$$

Following a diabatic transformation using the matrix $\mathbf{C}$

$$\begin{pmatrix}\langle\psi_D^0|\psi_D(t)\rangle & \langle\psi_D^0|\psi_A(t)\rangle\\ \langle\psi_A^0|\psi_D(t)\rangle & \langle\psi_A^0|\psi_A(t)\rangle\end{pmatrix} = \mathbf{C}^\dagger\begin{pmatrix}\langle\psi_{CD}^0|\psi_{CD}(t)\rangle & \langle\psi_{CD}^0|\psi_{CA}(t)\rangle\\ \langle\psi_{CA}^0|\psi_{CD}(t)\rangle & \langle\psi_{CA}^0|\psi_{CA}(t)\rangle\end{pmatrix}\mathbf{C} \quad (41)$$

$\langle\psi_D^0|\psi_A(t)\rangle$ is the off-diagonal term of the resultant matrix. Note that this same calculation can also be used to determine the overlap needed to calculate the PIET rate for the reverse process.

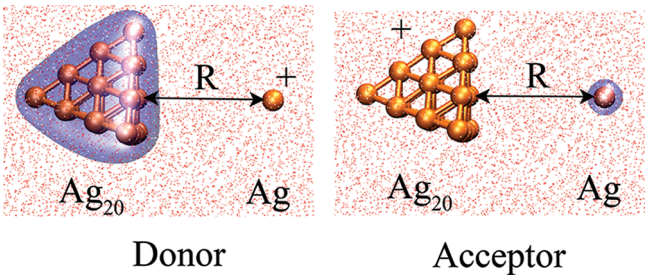

Figure 3. Model system consisting of a $(Ag_{20}-Ag)^+$ complex solvated in water. The density of transferring electron is indicated by the blue shade.

Finally, the PIET rate is written as

$$k_{PIET}(\omega) = \frac{2\pi}{\hbar}\frac{e^{-(-\Delta G_0 - \hbar\omega + \lambda_1)^2/4\lambda_1 k_B T}}{\sqrt{4\pi\lambda_1 k_B T}}\mu_{DA}^2(\omega)\frac{I(\omega)}{c\varepsilon_0} \quad (42)$$

and the linear relation between $k_{PIET}(\omega)$ and $I(\omega)$ allows us to define a PIET cross section, $\sigma_{PIET}(\omega)$

$$\sigma_{PIET}(\omega) = \hbar\omega\frac{k_{PIET}(\omega)}{I(\omega)} = \frac{2\pi\omega}{c\varepsilon_0}\frac{e^{-(-\Delta G_0 - \hbar\omega + \lambda_1)^2/4\lambda_1 k_B T}}{\sqrt{4\pi\lambda_1 k_B T}}\mu_{DA}^2(\omega) \quad (43)$$

This cross section is useful for quantifying the efficiency of electron transfer. In particular, the conversion rate from photons to electrons can be also represented by the quantum yield (QY)

$$QY(\omega) = \frac{\sigma_{PIET}(\omega)}{\sigma_{abs}(\omega) + \sigma_{PIET}(\omega)} \quad (44)$$

where $\sigma_{abs}(\omega)$ is the absorption cross section defined as the ratio between the stimulated transition rate and the incident photo flux density. The detailed protocol to evaluate $\sigma_{abs}(\omega)$ is given in ref 52.

So far, our discussions have been focused on the coherent transition rate from one diabatic ground state to another via the excited states. However, the so-called excited state ET rate, $k_e(\omega)$, can also be evaluated using this formalism. This is the quantity that is often measured using the transient absorption spectroscopy,[69] and in contrast to the PIET process it imagines that the excited state lives long enough that the population of excited states is well-defined. In our notation, $k_e(\omega)$ is the transition rate from Ψ_m to Ψ_D

$$k_e(\omega) = \frac{2\pi}{\hbar}(DWFC)\langle\psi_D^0|\hat{H}_0|\psi_m\rangle^2 = \frac{2\pi}{\hbar}\frac{\sigma_{PIET}(\omega)}{\sigma_{abs}(\omega)}\Gamma \quad (45)$$

Therefore, by calculating the ratio of $\sigma_{PIET}(\omega)$ and $\sigma_{abs}(\omega)$, we can determine the value of $k_e(\omega)$. Note that in our real-time formalism, this rate constant refers to the average over all excited states within the approximate energy width of Γ. Except for that, this rate constant does not explicitly depend on the excited state lifetime.

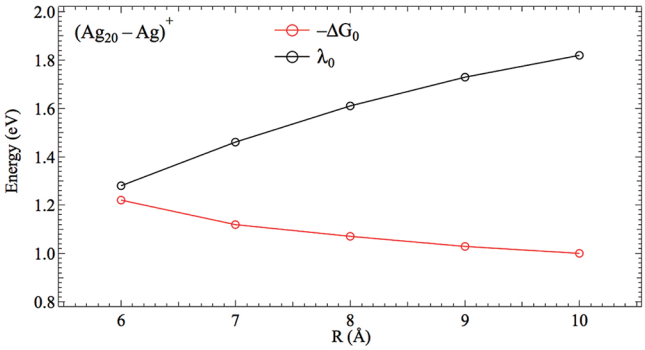

Figure 4. Ground state driving force and reorganization energy as a function of $Ag_{20}-Ag$ separation.

4. APPLICATION TO PIET FOR THE $(Ag_{20}-Ag)^+$ COMPLEX

a. Simulation Details. Our model system is a water-solvated $(Ag_{20}-Ag)^+$ complex consisting of a tetrahedral Ag_{20} cluster and an isolated Ag atom or ion (Figure 3). This system provides a simple model of a plasmonic silver nanoparticle (modeled as Ag_{20} based on past work[70,71] which shows this has plasmonic-like properties) interacting with a silver atom or ion in solution. Motivated by experimental work with much larger silver particles which shows plasmon-assisted reduction of silver ions in solution,[72,73] we will use this system to study plasmon-assisted electron transfer, with emphasis on whether the wavelengths that optimize PIET are similar to those which optimize absorption. Note that the thermodynamics of our model system looks like that in Figure 2 in which the donor is $Ag_{20}-Ag^+$ and the acceptor is Ag_{20}^+-Ag. The PIET process in this case involves oxidation of the Ag atom to Ag^+.

With this model system and the optical excitation, we will study the PIET rate between Ag_{20}^+ and Ag driven by the reorientation of the solvent as described by the Poisson–Boltzmann implicit solvation model.[74] A charge distribution function, Q_C, is defined to facilitate numerical definition of the diabatic states

$$Q_C = Q_{Ag_{20}} - Q_{Ag} \quad (46)$$

where $Q_{Ag_{20}}$ and Q_{Ag} are the charges of Ag_{20} and Ag, respectively. According to their relative energies, $Ag_{20}-Ag^+$ is the donor with $Q_D = -1$, whereas Ag_{20}^+-Ag is the acceptor with $Q_A = +1$. To examine the effect of donor–acceptor distance on the PIET rate, the separation from Ag to one of the triangular surfaces of Ag_{20} is varied from 6 to 10 Å equally spaced by 1 Å. The nuclei are otherwise fixed as we imagine that there are negligible structural changes associated with the electron transfer.

The APBS package[74] was utilized to solve the Poisson–Boltzmann equation to obtain the solvation potential (eq 8), a crucial component used in evaluating ΔG_0, λ_0, and λ_1. A dielectric constant of 78.54 and a molecular radius of 1.4 Å were chosen for the implicit water model, while the Blöchl scheme[75] was employed to determine the atomic charges of the explicit solute based on ground state electronic wave functions from the C-DFT calculations. The basic idea of the Blöchl scheme is to use localized atom-centered Gaussian packets to fit the multipole moments and the charge widths of a given electron density distribution, making it an excellent choice for charge fitting

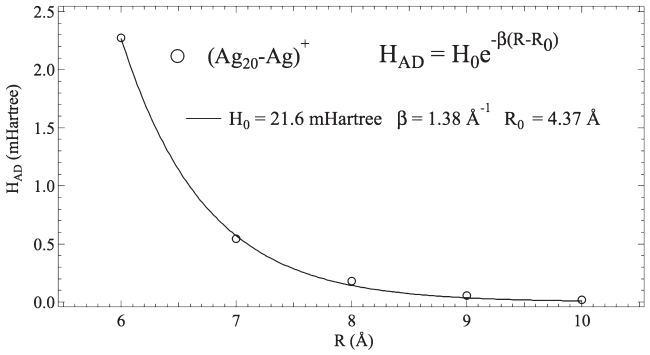

Figure 5. Exponential decay of the ground state electronic coupling strength.

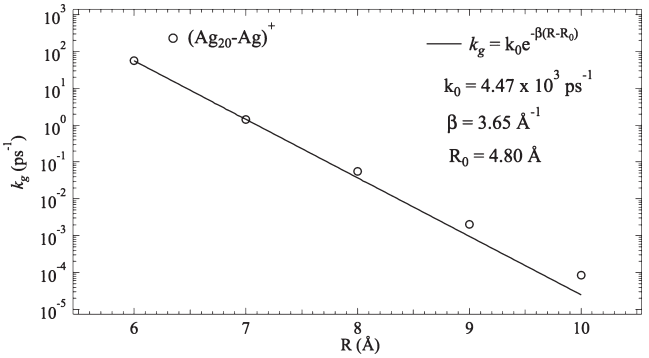

Figure 6. Computed ground state ET rates.

of optical properties that are subject to the multipole-field interactions.

The DFT, C-DFT, and C-RT-TDDFT calculations were all performed using the CP2K software[76] with the Perdeww−Burke−Ernzerhof (PBE) exchange-correlation functional,[77] the Goedecker−Teter−Hutter (GTH) pseudopotential[78] and the polarized-valence-double-ζ (PVDZ) basis set.[79] The geometry of Ag_{20} was first optimized by DFT with zero net charge, and then the ionized *Ag* was added along the *x* axis. In the CDFT calculation (eq 10), the constrained wave function optimization continued until a deviation from the target Q_C is less than 10^{-6}. Afterward, the optimized wave functions were used as the initial states in the C-RT-TDDFT simulations (eq 40), in which a short electric pulse E_x with a duration of 0.0121 fs and a field strength of 1.47×10^6 V/m was applied along the *x* axis to drive the electron dynamics. No polarization averaging is used in the present study. The time-dependent Schrödinger equation was integrated by the enforced-time-reversible-symmetry (ETRS) algorithm[80] with a time step of 0.0121 fs. A RT-TDDFT trajectory was propagated for a total of 4000 steps to converge all optical and ET properties using a value of 0.1 eV for the damping factor Γ. (This choice has often been used to empirically represent damping in a plasmonic system with frozen nuclei.[70,81,82]) The average solar radiation intensity of 342 Watt/m^2[83] was chosen to evaluate k_{PIET}. This value is in the range where linear optical response should occur.

b. Ground State ET Rate, k_g, for the Reaction $Ag_{20} + Ag^+ \rightarrow Ag_{20}^+ + Ag$. As shown in Figure 4, the magnitude of ΔG_0 decreases slightly from ∼1.2 to ∼1.0 eV when *R* is increased from 6 to 10 Å. This small change reflects the size of electrostatic interactions between the ion and polarizable atom for the

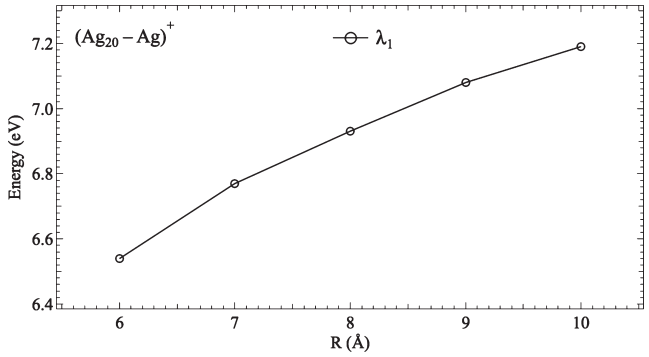

Figure 7. Reorganization energy of the donor.

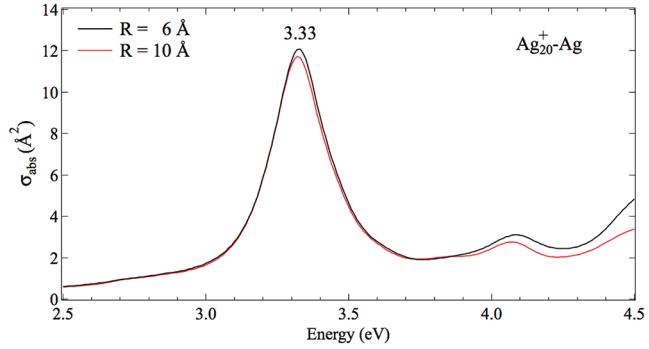

Figure 8. Calculated absorption cross section of Ag_{20}^+−Ag.

distances considered. By contrast, λ_0 was found to increase substantially by ∼0.5 eV over the same range of *R*, as the separated Ag_{20}^+ and Ag^+ are more strongly solvated than the merged complex. The optimum condition of Marcus theory, i.e., $-\Delta G_0 = \lambda_0$, almost occurs at $R = 6$ Å, leading to a sizable DWFC.

The calculated H_{DA}^0 is presented in Figure 5. This exhibits a rapid decay with increasing *R* due to the exponential variation of the overlap of electronic wave functions.[84] By fitting it to a shifted exponential function of the form of

$$H_{AD}^0 = H_0 e^{-\beta(R - R_0)} \quad (47)$$

the value 1.38 Å^{-1} is obtained for the decay coefficient, β. Compared to the DBA systems which typically have $\beta < 0.6$ Å^{-1},[25] the more rapid variation of H_{DA}^0 in our $(Ag_{20}-Ag)^+$ complex is likely caused by the absence of a π-conjugated bridge molecule.

Using the Marcus formalism of eq 1, and H_{DA}^0 from Figure 5, the ground state rate k_g at 300 K is shown in Figure 6. Not surprisingly the exponential decay law is again satisfied, this time with an even larger value of 3.65 Å^{-1} for β due to the presence of $|H_{DA}^0|^2$ (Figure 5) in eq 1 and the dependence of ΔG_0 and λ_0 on *R* (Figure 4) in the exponent on the right side of eq 1. For $R < 8$ Å, ground state ET occurs on the picosecond time scale, which means that it is faster than significant structural relaxation. When $R > 9$ Å, k_g drops to the nanosecond time scale that is comparable with large-scale nuclear motions.

c. PIET Rate, $k_{PIET}(\omega)$, for the Reaction $Ag_{20}^+ + Ag \xrightarrow{h\nu} Ag_{20} + Ag^+$. The excited state ET rate uses the reorganization energy λ_1, which is plotted in Figure 7. As expected, the reorganization energy increases with Ag_{20}−Ag separation much as with λ_0. However, λ_1 is much larger than λ_0 because of the larger

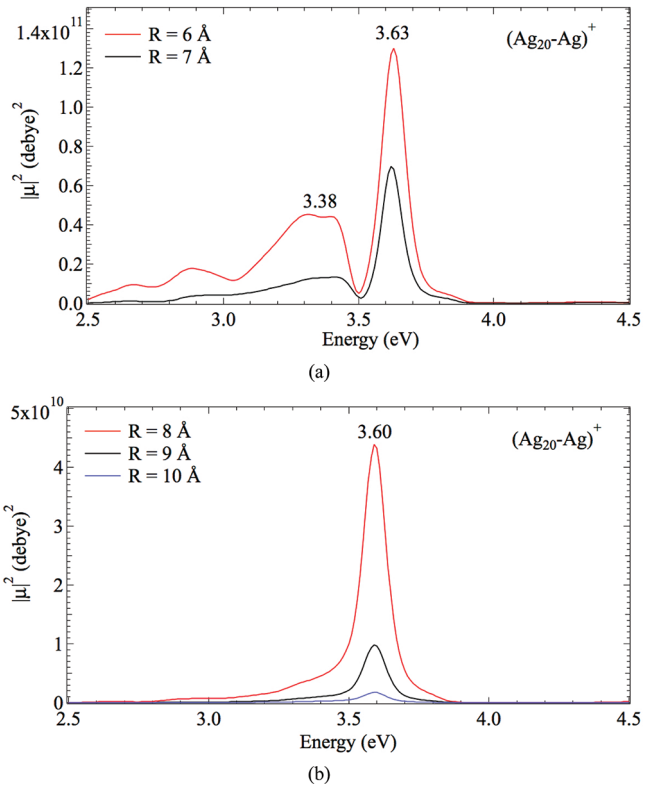

Figure 9. Squared magnitude of the PIET matrix element, $|\mu|^2$.

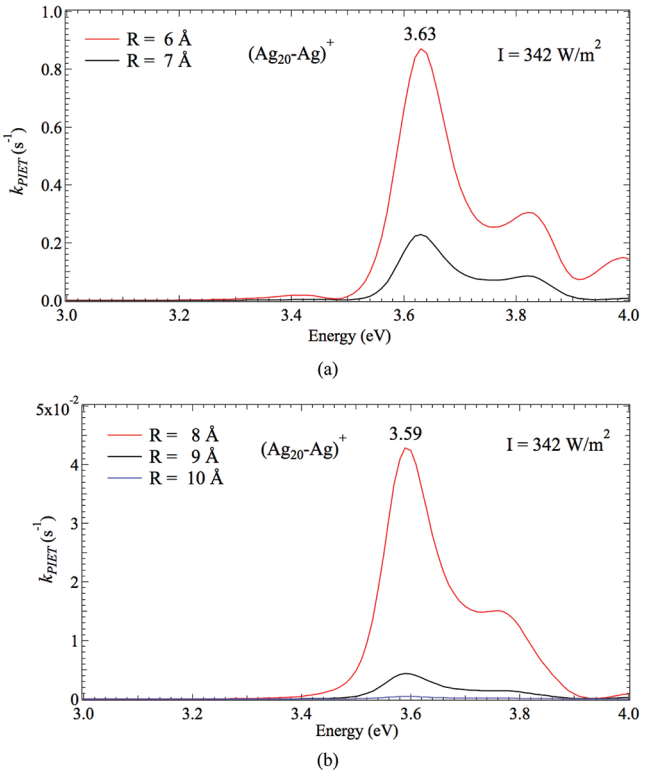

Figure 10. PIET rates, $k_{\mathrm{PIET}}(\omega)$.

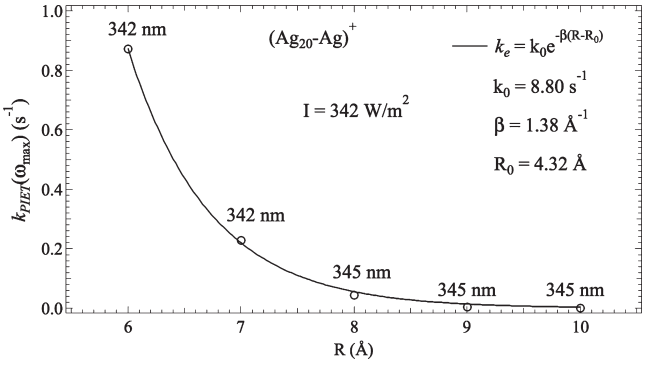

Figure 11. Maximum k_{PIET} as a function of R. The PIET resonance wavelengths used to calculate k_{PIET} are given under the circle markers.

solvation energy of the isolated Ag^+ than that of Ag_{20}^+, in which the extra positive charge is delocalized over the whole cluster. This higher reorganization energy exceeds the PIET driving force, $-\Delta G_0 - \hbar\omega$, even in the visible spectrum, and as a result the PIET rate is relatively slow for solar incident flux (see below).

In our derivation of the PIET rate, the excited molecular orbitals are assumed to provide the essential intermediate states for the stepwise ET relay. To quantitatively reveal the relation between light absorption and PIET, the absorption cross section $\sigma_{\mathrm{abs}}(\omega)$ of the irradiated acceptor Ag_{20}^+−Ag is shown in Figure 8. For visual simplicity, only results for 6 and 10 Å are presented. Nevertheless, the two spectra are nearly identical with a sharp intraband peak centered at 3.33 eV in addition to a broad plateau to the blue. The peak location is in good agreement with a previous theoretical study using frequency domain TDDFT on Ag_{20}.[71] Note that this transition can be thought of as defining a plasmon-like excitation which for larger clusters becomes the plasmon-resonance excitation. For the Ag_{20}^+−Ag system, the invariance of the spectrum to the location of the Ag atom indicates that electronic excitation predominantly occurs in the Ag_{20}^+ moiety, with little influence from the Ag. This can be understood since the lowest excitation energy of silver atom is well above that for Ag_{20}^+.

The squared magnitude of the frequency-dependent PIET matrix element, $|\mu|^2$, calculated by C-RT-TDDFT is plotted as a function of frequency in Figure 9. For small separations $R \leq 7$ Å, there exists a flat plateau centered at ∼3.38 eV, in addition to a sharp primary peak at ∼3.63 *eV*. It is very interesting to note that $|\mu|^2$ does not maximize at the absorption maximum (3.33 eV in Figure 8), suggesting that molecular orbitals with high oscillator strength are not the most effective in producing electron transfer. This hypothesis is even more apparent in the appearance of $|\mu|^2$ at larger separations $R \geq 8$ Å where the flat plateau nearly disappears, leaving a peak at ∼3.60 eV as the only feature. Note also that the primary peak height decreases significantly from 1.4×10^{11} to 1.7×10^{9} debye^2 as R increases from 6 to 10 Å, corresponding to an approximately equivalent to 5-fold reduction for every angstrom of additional separation.

Assuming an incident intensity of 342 W/m^2, the calculated k_{PIET} is shown in Figure 10. This demonstrates a similar frequency dependence to $|\mu|^2$ except for a notable increase toward the blue. This arises because the maximum DWFC occurs in the UV, i.e., $\hbar\omega$ = 8.0 eV. By plotting the maximum k_{PIET} (near 3.6 eV) as a function of R, and fitting it to a shifted exponential function (Figure 11), a smaller value of 1.38 Å^{-1} for β is found in comparison to 3.65 Å^{-1} in k_g. The slower decay in

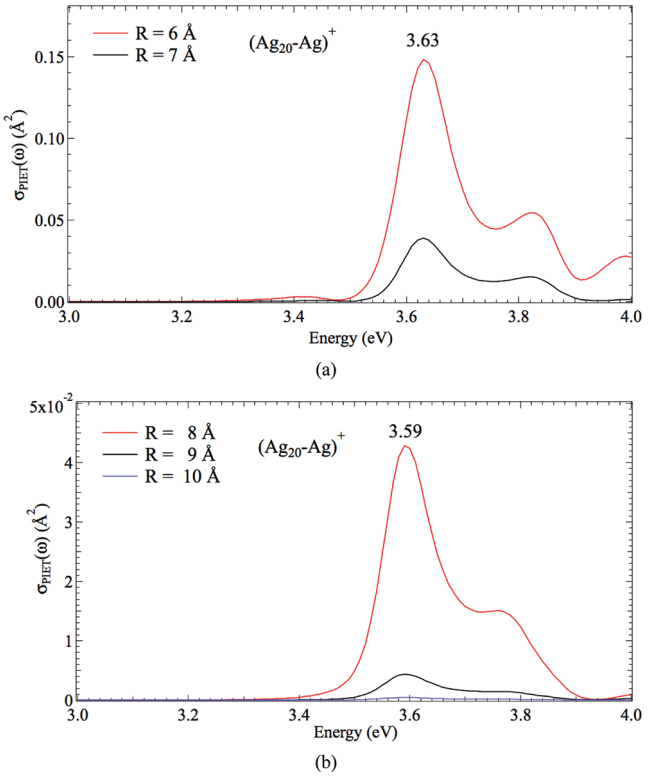

Figure 12. Frequency-dependent PIET cross section, $\sigma_{PIET}(\omega)$.

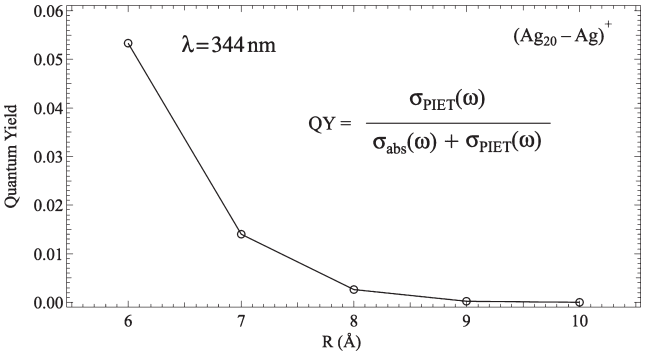

Figure 13. Quantum yield at the PIET resonance wavelength of 344 nm as a function of R.

ET rate with R for photoexcited states is a consequence of the stronger Hamiltonian coupling as induced by spatially more extended molecular orbitals.

The PIET cross section, $\sigma_{PIET}(\omega)$, is shown in Figure 12 and exhibits a similar pattern to $\sigma_{abs}(\omega)$, yet with a much smaller resonant magnitude even for small separations. For instance, when R = 6 Å, $\sigma_{PIET}(\omega)$ at $\hbar\omega$ = 3.63 eV is approximately 20 times smaller than $\sigma_{abs}(\omega)$ at $\hbar\omega$ = 3.33 eV, suggesting that the $(Ag_{20}{-}Ag)^+$ complex is still much more efficient in aiding vertical excitation than facilitating parallel ET when its two components are narrowly separated. For the largest separation of R = 10 Å, the ratio between $\sigma_{PIET}(\omega)$ and $\sigma_{abs}(\omega)$ significantly decreases to 10^{-5}, essentially shutting-off electron transfer. The rather low PIET efficiency is also exhibited in Figure 13, which presents the quantum yield at $\hbar\omega$ = 3.60 eVas a function of R. It

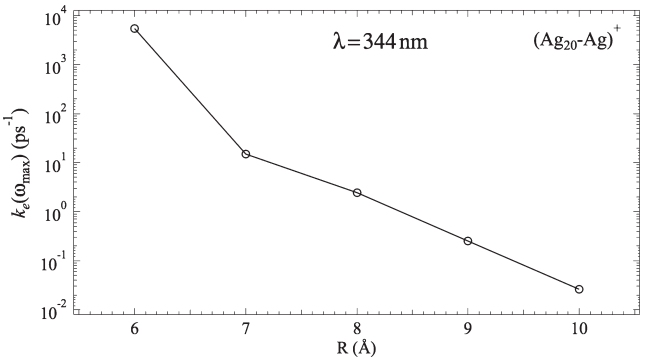

Figure 14. Excited state ET rate, k_e, at the PIET resonance wavelength of 344 nm as a function of R.

turns out that at most 5% of the light energy can be transferred into electrons R = 6 Å even for the optimal wavelength of 344 nm.

At the same incident wavelength, the excited state ET rate constant, $k_e(\omega)$, shows a dramatic decay with distance from fs^{-1} at R = 6 Å to ns^{-1} at R = 10 Å (Figure 14). The reason why the excited state rate constant is so dramatically larger than the PIET rate constant can be understood by examining eqs 33 and 45. This shows that the ratio of the PIET and excited state rates involves light intensity multiplied by dipole matrix element squared and divided by the excited state width. In the present application, the width factor corresponds to decay in 40 fs, so given the weak light intensity, the population of excited states capable of undergoing electron transfer is extremely small. To make the rates more comparable would require intensities that are 12 orders of magnitude higher.

5. DISCUSSION AND CONCLUSION

We have developed a real-time TDDFT approach for calculating rates of photoinduced electron transfer and have demonstrated its use in describing PIET for a plasmonic-like model corresponding to oxidation/reduction of Ag/Ag^+ near a silver cluster. C-DFT was first employed to construct the diabatic ground states for donor and acceptor, from which the driving force and solvent reorganization energies were obtained in combination with an implicit solvent model. To describe PIET, an external electric field is applied to the diabatic ground states and the time-dependent Kohn−Sham equation is solved to determine donor and acceptor wave functions. By calculating the time evolution of the diabatic wave function overlap, the PIET cross section in the frequency domain is readily determined through a Fourier transform. For reference, we have also determined absorption cross sections using a related real-time approach so that the relative efficiencies of these two processes could be compared.

In our application to the $(Ag_{20}{-}Ag)^+$ complex, C-RT-TDDFT shows a plasmonic-like absorption spectrum, which peaks at 3.33 eV, similar to what has been found in past studies of Ag_{20}. For the PIET cross section, a sharp primary peak is found at ∼3.60 eV for all donor−acceptor separations, indicating that excitation which optimizes PIET is distinct from excitation which optimizes absorption. The PIET cross section $\sigma_{PIET}(\omega)$ is found to be 0.15 $Å^2$ for R = 6 Å and ∼3.63 eV, which is only about 5% of the absorption cross section, indicating that PIET is a small component of the overall light absorbed by the silver cluster. In addition, the quantum efficiency of PIET undergoes a significant 4-fold reduction at

R = 7 Å due to the diminished electronic coupling strength as the donor and acceptor move apart. Overall this shows that PIET is very inefficient for the silver cluster system, and this is primarily due to strong damping which occurs for plasmonic systems.

From a technical perspective, the most striking advantage of the C-RT-TDDFT approach is the elimination of the explicit construction of the excited states, which are the major sources of CPU consumption and memory allocation in most excited state simulations. On the theory side, the optimum scheme to impose charge constraints for excited states is not yet clear as C-DFT was originally developed for the diabatic ground states.[37] By dealing with the response of the diabatic ground states to external electromagnetic perturbation, C-RT-TDDFT avoids this ambiguity and determines the electronic coupling strength at no additional cost compared to ground state simulations. As a result, C-RT-TDDFT enables the investigation of PIET on systems with hundreds of atoms, large enough to cover most organic electronics of interest. Moreover, C-DFT is in principle a modified ground state approach that eliminates the necessity of constructing the localized ET states from the dubiously defined unoccupied Kohn−Sham orbitals. Thus, the time propagation of the charge constrained states in C-RT-TDDFT is more likely to imitate the diabatic state evolution than the unconstrained RT-TDDFT, which usually starts from a mixture of the occupied and unoccupied Kohn−Sham orbitals. Nevertheless, several assumptions are made in our development that might limit its applicability, including neglect of structural relaxation upon electronic excitation, and neglect of internal conversion that competes with excited state ET.[85] Several studies have already been carried out to estimate the nonradiative decay rate,[86−88] and their incorporation into our approach is an important future direction. Another possible limitation of the C-RT-TDDFT comes from the single-determinant and single-particle characteristics of the Kohn−Sham orbitals, which usually fail to capture the static part of the electron correlation when there are nearly degenerate electron configurations.[89] However, a configuration interaction (CI) based C-DFT study has shown that the missing static correlation of the localized diabatic states can be partially recovered through a multireference active space, suggesting a promising solution to extend C-RT-TDDFT for investigating PIET in strongly correlated systems.[90]

As a fundamental chemical process, PIET is important in numerous chemical, biological and medical applications[91−93] where damping effects are less important than in the present application. However because the damping is less important, longer calculations will be required. Thus the theoretical modeling of PIET remains a challenging yet rewarding task as light radiation offers unique opportunities for control over ET. Indeed, coherent control[94,95] has become a powerful tool for selectively breaking or forming chemical bonds using multiple laser pulses shorter than the molecular vibrational period, and its application to PIET could be explored using our approach. Also, since C-RT-TDDFT does not impose any limitations on the number of perturbed electric fields and their amplitudes, frequencies, shapes, and durations, it is an excellent choice for the investigation of nonlinear control.

AUTHOR INFORMATION

Corresponding Author

Fax: 847-491-7713. Phone: 847-491-5657. E-mail: schatz@chem.northwestern.edu.

ACKNOWLEDGMENT

The research was supported by Grant DE-SC0004752 funded by the U.S. Department of Energy, Office of Science and Office of Basic Energy Sciences. The computational resources utilized in this research were provided by Shanghai Supercomputer Center.

REFERENCES

(1) Freeman, G. R. *Annu. Rev. Phys. Chem.* **1983**, *34*, 463–492.
(2) Kestner, N. R.; Logan, J.; Jortner, J. *J. Phys. Chem.* **1974**, *78*, 2148–2166.
(3) Piotrowiak, P. *Chem. Soc. Rev.* **1999**, *28*, 143–150.
(4) Gray, H. B.; Winkler, J. R. *Annu. Rev. Biochem.* **1996**, *65*, 537–561.
(5) Moore, G. R.; Huang, Z.-X.; Eley, C. G. S.; Barker, H. A.; Williams, G.; Robinson, M. N.; Williams, R. J. P. *Faraday Discuss. Chem. Soc.* **1982**, *74*, 311–329.
(6) Boyer, P. D. *Annu. Rev. Biochem.* **1997**, *66*, 717–749.
(7) Capaldi, R. A. *Annu. Rev. Biochem.* **1990**, *59*, 569–596.
(8) Michel, B.; Bosshard, H. R. *J. Biol. Chem.* **1984**, *259*, 10085–10091.
(9) Regan, J. J.; Ramirez, B. E.; Winkler, J. R.; Gray, H. B.; Malmström, B. G. *J. Bioenerg. Biomembr.* **1998**, *30*, 35–39.
(10) Kaila, V. R. I.; Johansson, M. P.; Sundholm, D.; Wikström, M. *Proc. Natl. Acad. Sci.* **2010**, *107*, 21470–21475.
(11) Yu, L. H.; Keane, Z. K.; Ciszek, J. W.; Cheng, L.; Stewart, M. P.; Tour, J. M.; Natelson, D. *Phys. Rev. Lett.* **2004**, *93*, 266802–266805.
(12) Galperin, M.; Ratner, M. A.; Nitzan, A. *J. Chem. Phys.* **2004**, *121*, 11965–11979.
(13) Troisi, A.; Ratner, M. A. *Small* **2006**, *2*, 172–181.
(14) Kwiatkowski, J. J.; Frost, J. M.; Kirkpatrick, J.; Nelson, J. *J. Phys. Chem. A.* **2008**, *112*, 9113–9117.
(15) Franzen, S.; Martin, J. *Annu. Rev. Phys. Chem.* **1995**, *46*, 453–488.
(16) Potasek, M. J.; Hopfield, J. J. *Proc. Natl. Acad. Sci.* **1977**, *74*, 3817–3820.
(17) Gould, I. R.; Young, R. H.; Mueller, L. J.; Albrecht, A. C.; Farid, S. *J. Am. Chem. Soc.* **1994**, *116*, 3147–3148.
(18) Bahr, J. L.; Kuciauskas, D.; Liddell, P. A.; Moore, A. L.; Moore, T. A.; Gust, D. *Photochem. Photobiol.* **2000**, *72*, 598–611.
(19) Kee, T. W.; Son, D. H.; Kambhampati, P.; Barbara, P. F. *J. Phys. Chem. A* **2001**, *105*, 8434–8439.
(20) Dexter, D. L. *J. Chem. Phys.* **1953**, *21*, 836–850.
(21) McConnell, H. M. *J. Chem. Phys.* **1961**, *35*, 508–515.
(22) Anderson, P. W. *Phys. Rev.* **1950**, *79*, 350–356.
(23) Ratner, M. A. *J. Phys. Chem.* **1990**, *94*, 4877–4883.
(24) Wasielewski, M. R. *Chem. Rev.* **1992**, *92*, 435–461.
(25) Lewis, F. D.; Wu, T.; Zhang, Y.; Letsinger, R. L.; Greenfield, S. R.; Wasielewski, M. R. *Science* **1997**, *277*, 673–676.
(26) Anderson, N. A.; Ai, X.; Chen, D.; Mohler, D. L.; Lian, T. *J. Phys. Chem. B.* **2003**, *107*, 14231–14239.
(27) Closs, G. L.; Calcaterra, L. T.; Green, N. J.; Penfield, K. W.; Miller, J. R. *J. Phys. Chem.* **1986**, *90*, 3673–3683.
(28) Turró, C.; Zaleski, J. M.; Karabatsos, Y. M.; Nocera, D. G. *J. Am. Chem. Soc.* **1996**, *118*, 6060–6067.
(29) Tvrdy, K.; Frantsuzov, P. A.; Kamat, P. V. *Proc. Natl. Acad. Sci.* **2011**, *108*, 29–34.
(30) Tavernier, H. L.; Barzykin, A. V.; Tachiya, M.; Fayer, M. D. *J. Phys. Chem. B.* **1998**, *102*, 6078–6088.
(31) Fukuzumi, S.; Ohkubo, K.; E, W.; Ou, Z.; Shao, J.; Kadish, K. M.; Hutchison, J. A.; Ghiggino, K. P.; Sintic, P. J.; Crossley, M. J. *J. Am. Chem. Soc.* **2003**, *125*, 14984–14985.
(32) Marcus, R. A. *Annu. Rev. Phys. Chem.* **1964**, *15*, 155–196.
(33) Jortner, J. *J. Chem. Phys.* **1976**, *64*, 4860–4867.
(34) Mead, C. A.; Truhlar, D. G. *J. Chem. Phys.* **1982**, *77*, 6090–6098.
(35) Newton, M. D. *Int. J. Quantum Chem.* **2000**, *77*, 255–263.

(36) Wu, Q.; Van Voorhis, T. *J. Phys. Chem. A* **2006**, *110*, 9212–9218.
(37) Wu, Q.; Van Voorhis, T. *Phys. Rev. A* **2005**, *72*, 024502–024505.
(38) Perdew, J. P.; Zunger, A. *Phys. Rev. B* **1981**, *23*, 5048–5079.
(39) Huang, P.; Carter, E. A. *Annu. Rev. Phys. Chem.* **2008**, *59*, 261–290.
(40) Rudra, I.; Wu, Q.; Van Voorhis, T. *J. Chem. Phys.* **2006**, *124*, 024103–024109.
(41) Wu, Q.; Van Voorhis, T. *J. Chem. Theory Comput.* **2006**, *2*, 765–774.
(42) Perdew, J. P.; Parr, R. G.; Levy, M.; Balduz, J. L. *Phys. Rev. Lett.* **1982**, *49*, 1691–1694.
(43) Marques, M. A. L.; Gross, E. K. U. *Annu. Rev. Phys. Chem.* **2004**, *55*, 427–455.
(44) Dreuw, A.; Weisman, J. L.; Head-Gordon, M. *J. Chem. Phys.* **2003**, *119*, 2943–2946.
(45) Ghosh, P.; Gebauer, R. *J. Chem. Phys.* **2010**, *132*, 104102–104105.
(46) Yabana, K.; Bertsch, G. F. *Phys. Rev. B* **1996**, *54*, 4484–4487.
(47) Brabec, T.; Krausz, F. *Rev. Mod. Phys.* **2000**, *72*, 545–591.
(48) Marques, M. A. L.; Castro, A.; Bertsch, G. F.; Rubio, A. *Comput. Phys. Commun.* **2003**, *151*, 60–78.
(49) Schrödinger, E. R. J. A. *Phys. Rev.* **1926**, *28*, 1049–1070.
(50) Bertsch, G. F.; Iwata, J. I.; Rubio, A.; Yabana, K. *Phys. Rev. B* **2000**, *62*, 7998–8002.
(51) Takimoto, Y.; Vila, F. D.; Rehr, J. J. *J. Chem. Phys.* **2007**, *127*, 154114–154123.
(52) Chen, H.; McMahon, J. M.; Ratner, M. A.; Schatz, G. C. *J. Phys. Chem. C* **2010**, *114*, 14384–14392.
(53) Meng, S.; Kaxiras, E. *J. Chem. Phys.* **2008**, *129*, 054110–054121.
(54) Yabana, K.; Nakatsukasa, T.; Iwata, J. I.; Bertsch, G. F. *Phys. Status Solidi B* **2006**, *243*, 1121–1138.
(55) Burnus, T.; Marques, M. A. L.; Gross, E. K. U. *Phys. Rev. A.* **2005**, *71*, 010501–010504.
(56) Kurth, S.; Stefanucci, G.; Almbladh, C. O.; Rubio, A.; Gross, E. K. U. *Phys. Rev. B.* **2005**, *72*, 035308–035320.
(57) Qian, X.; Li, J.; Lin, X.; Yip, S. *Phys. Rev. B* **2006**, *73*, 035408–035418.
(58) Van Voorhis, T.; Kowalczyk, T.; Kaduk, B.; Wang, L.-P.; Cheng, C.-L.; Wu, Q. *Annu. Rev. Phys. Chem.* **2010**, *61*, 149–170.
(59) Cheng, C.-L.; Evans, J. S.; Van Voorhis, T. *Phys. Rev. B* **2006**, *74*, 155112–155122.
(60) Miyamoto, Y.; Rubio, A.; Tománek, D. *Phys. Rev. Lett.* **2006**, *97*, 126104–126107.
(61) Grätzel, M. *J. Photochem. Photobiol., C: Photochem. Rev.* **2003**, *4*, 145–153.
(62) Dulicacute, D.; van der Molen, S. J.; Kudernac, T.; Jonkman, H. T.; de Jong, J. J. D.; Bowden, T. N.; van Esch, J.; Feringa, B. L.; van Wees, B. J. *Phys. Rev. Lett.* **2003**, *91*, 207402–207405.
(63) Kudo, A.; Miseki, Y. *Chem. Soc. Rev.* **2009**, *38*, 253–278.
(64) Marcus, R. A.; Sutin, N. *Biochim. Biophys. Acta, Bioenerg.* **1985**, *811*, 265–322.
(65) Dance, Z. E. X.; Mickley, S. M.; Wilson, T. M.; Ricks, A. B.; Scott, A. M.; Ratner, M. A.; Wasielewski, M. R. *J. Phys. Chem. A.* **2008**, *112*, 4194–4201.
(66) Claude, J. P.; Meyer, T. J. *J. Phys. Chem.* **1995**, *99*, 51–54.
(67) Wu, Q.; Van Voorhis, T. *J. Chem. Phys.* **2006**, *125*, 164105–164113.
(68) Kohn, W.; Sham, L. J. *Phys. Rev.* **1965**, *140*, A1133–A1138.
(69) She, C.; Lee, S. J.; McGarrah, J. E.; Vura-Weis, J.; Wasielewski, M. R.; Chen, H.; Schatz, G. C.; Ratner, M. A.; Hupp, J. T. *Chem. Commun.* **2010**, *46*, 547–549.
(70) Zhao; Jensen, L.; Schatz, G. C. *J. Am. Chem. Soc.* **2006**, *128*, 2911–2919.
(71) Aikens, C. M.; Li, S.; Schatz, G. C. *J. Phys. Chem. C* **2008**, *112*, 11272–11279.
(72) Jin, R.; Cao, Y.; Mirkin, C. A.; Kelly, K. L.; Schatz, G. C.; Zheng, J. G. *Science* **2001**, *294*, 1901–1903.
(73) Jin, R.; Cao, Y. C.; Hao, E.; Metraux, G. S.; Schatz, G. C.; Mirkin, C. A. *Nature* **2003**, *425*, 487–490.
(74) Baker, N. A.; Sept, D.; Joseph, S.; Holst, M. J.; McCammon, J. A. *Proc. Natl. Acad. Sci.* **2001**, *98*, 10037–10041.
(75) Blochl, P. E. *J. Chem. Phys.* **1995**, *103*, 7422–7428.
(76) VandeVondele, J.; Krack, M.; Mohamed, F.; Parrinello, M.; Chassaing, T.; Hutter, J. *Comput. Phys. Commun.* **2005**, *167*, 103–128.
(77) Perdew, J. P.; Burke, K.; Ernzerhof, M. *Phys. Rev. Lett.* **1996**, *77*, 3865–3868.
(78) Goedecker, S.; Teter, M.; Hutter, J. *Phys. Rev. B* **1996**, *54*, 1703–1710.
(79) Woon, D. E.; Dunning, J. T. H. *J. Chem. Phys.* **1994**, *100*, 2975–2988.
(80) Castro, A.; Marques, M. A. L.; Rubio, A. *J. Chem. Phys.* **2004**, *121*, 3425–3433.
(81) Jensen, L.; Autschbach, J.; Schatz, G. C. *J. Chem. Phys.* **2005**, *122*, 224115–224125.
(82) Jensen, L.; Aikens, C. M.; Schatz, G. C. *Chem. Soc. Rev.* **2009**, *37*, 1061–1073.
(83) McIntosh, D. H. *Q. J. R. Meteorol. Soc.* **1978**, *104*, 534–534.
(84) Barbara, P. F.; Meyer, T. J.; Ratner, M. A. *J. Phys. Chem.* **1996**, *100*, 13148–13168.
(85) Hare, P. M.; Crespo-Hernández, C. E.; Kohler, B. *Proc. Natl. Acad. Sci.* **2007**, *104*, 435–440.
(86) Barqawi, K. R.; Murtaza, Z.; Meyer, T. J. *J. Phys. Chem.* **1991**, *95*, 47–50.
(87) Habenicht, B. F.; Prezhdo, O. V. *J. Phys. Chem. C* **2009**, *113*, 14067–14070.
(88) Meng, S.; Kaxiras, E. *Biophys. J.* **2008**, *95*, 4396–4402.
(89) Cremer, D. *Mol. Phys.* **2001**, *99*, 1899–1940.
(90) Wu, Q.; Cheng, C.-L.; Van Voorhis, T. *J. Chem. Phys.* **2007**, *127*, 164119–164128.
(91) Marcus, R. A. *Rev. Mod. Phys.* **1993**, *65*, 599–610.
(92) Reece, S. Y.; Nocera, D. G. *Annu. Rev. Biochem.* **2009**, *78*, 673–699.
(93) DiCesare, N.; Lakowicz, J. R. *J. Biomed. Opt.* **2002**, *7*, 538–545.
(94) Brumer, P.; Shapiro, M. *Annu. Rev. Phys. Chem.* **1992**, *43*, 257–282.
(95) Ohmori, K. *Annu. Rev. Phys. Chem.* **2009**, *60*, 487–511.